

manuscript submitted to *JGR-Space Physics*

1 Bayesian filtering in incoherent scatter plasma 2 parameter fits

3 **Ilkka I. Virtanen¹, Habtamu W. Tesfaw¹, Lassi Roininen², Sari Lasanen³, and**
4 **Anita Aikio¹**

5 ¹Space Physics and Astronomy Research Unit, University of Oulu, Oulu, Finland

6 ²School of Engineering Science, Lappeenranta-Lahti University of Technology, Lappeenranta, Finland

7 ³Sodankylä Geophysical Observatory, University of Oulu, Sodankylä, Finland

8 **Key Points:**

- 9 Full-profile incoherent scatter analysis is implemented by means of Bayesian fil-
10 tering and correlation priors.
- 11 The technique reaches high time resolutions and enables ion composition fits.
- 12 We have implemented the technique as an additional module to the GUISDAP
13 incoherent scatter analysis tool.

Corresponding author: Ilkka I. Virtanen, ilkka.i.virtanen@oulu.fi

14 **Abstract**

15 Incoherent scatter (IS) radars are invaluable instruments for ionospheric physics, since
 16 they observe altitude profiles of electron density (N_e), electron temperature (T_e), ion tem-
 17 perature (T_i) and line-of-sight plasma velocity (V_i) from ground. However, the temper-
 18 atures can be fitted to the observed IS spectra only when the ion composition is known,
 19 and resolutions of the fitted plasma parameters are often insufficient for auroral electron
 20 precipitation, which requires high resolutions in both range and time. The problem of
 21 unknown ion composition has been addressed by means of the full-profile analysis, which
 22 assumes that the plasma parameter profiles are smooth in altitude, or follow some pre-
 23 defined shape. In a similar manner, one could assume smooth time variations, but this
 24 option has not been used in IS analysis. We propose a plasma parameter fit technique
 25 based on Bayesian filtering, which we have implemented as an additional Bayesian Fil-
 26 tering Module (BAFIM) in the GUISDAP analysis package. BAFIM allows us to con-
 27 trol gradients in both time and range directions for each plasma parameter separately.
 28 With BAFIM we can fit F_1 region ion composition together with N_e , T_e , T_i and V_i , and
 29 we have reached 4 s/900 m time/range steps in four-parameter fits of N_e , T_e , T_i and V_i
 30 in E region observations of auroral electron precipitation.

31 **1 Introduction**

32 Incoherent scatter (IS) radars are high-power, large-aperture radars that detect ra-
 33 dio wave scattering from thermal fluctuations in the ionospheric plasma. Power spec-
 34 tral density of the scattered signal is a function of number density, temperature, bulk
 35 velocity, and ion-neutral collision frequency of a number of ion species and electrons (for
 36 example Swartz & Farley, 1979, and references therein). All these parameters cannot be
 37 fitted to the spectrum, and a commonly used approximation is the four-parameter fit of
 38 N_e , T_e , T_i and V_i . Equal temperatures and bulk velocities are assumed for all ion species,
 39 and the ion-neutral collision frequency and ion composition are taken from ionospheric
 40 models.

41 In the F_1 region the four-parameter fit often produces incorrect temperatures (for
 42 example Blelly & van Eyken, 2010), because ion composition models are unreliable in
 43 the transition region from the E region molecular NO^+ and O_2^+ ions to the F_2 region atomic
 44 O^+ . Incorrect compositions bias the temperatures, because the IS spectrum is sensitive
 45 to the ratio T_i/m_i , where m_i is the mean ion mass. This is known as the "temperature-
 46 ion composition ambiguity" (TICA) (Martínez-Ledesma et al., 2019). Several authors
 47 have addressed the TICA problem by means of modeling the F_1 region temperature and
 48 ion composition profiles (Kelly & Wickwar, 1981; Cabrit & Kofman, 1996; Blelly & van
 49 Eyken, 2010; Zettergren et al., 2011; Häggström & Collis, 1990). Also direct estimation
 50 of both ion composition and temperature has been reported by Lathuillere, Lejeune, and
 51 Kofman (1983), but coarse resolutions were used, since such fits require extremely ac-
 52 curate IS spectra (Martínez-Ledesma et al., 2019).

53 Even the four-parameter fits are extremely challenging with a few second and a few
 54 hundred meter resolutions that are needed in observations of auroral electron precipi-
 55 tation. In high-resolution observations one may replace the fitted N_e with the raw elec-
 56 tron density (scaled back-scattered power) N_r . For example Semeter and Kamalabadi
 57 (2005), Dahlgren et al. (2011), and Virtanen et al. (2018) used N_r in estimation of pri-
 58 mary energy spectra of precipitating electrons. However, N_r equals N_e only if $T_e = T_i$,
 59 which may be an unjustified assumption when the precipitation heats the electron gas.

60 We propose an IS analysis technique that combines Bayesian filtering (for exam-
 61 ple Säkkä, 2013) in time and correlation priors (Roininen et al., 2011) in range. The
 62 combination allows us to extend the idea of full-profile IS analysis (Holt et al., 1992; Lehti-
 63 nen et al., 1996; Hysell et al., 2008), which assumes smoothness in range, to an assump-
 64 tion of smoothness in both time and range. With this approach we can fit ion compo-

65 sitions if both ion temperature and composition are assumed to vary smoothly with time
66 and altitude, and we can include temperature fits in high-resolution electron density fits.

67 In Section 2 we give introduction to IS plasma parameter fits, Bayesian filtering
68 and correlation priors. In Section 3 we explain how the prior models and Bayesian fil-
69 tering are used in IS analysis and implemented as a 'Bayesian Filtering Module' (BAFIM)
70 in GUISDAP. In Section 4 we demonstrate BAFIM fits of N_e , T_e , T_i , V_i , and ion com-
71 position $p=[O^+]/N_e$ in the F₁ region, and high-resolution fits of N_e , T_e , T_i , and V_i in the
72 E region.

73 2 Theoretical background

74 Incoherent scatter signal from a small plasma volume is a zero-mean random pro-
75 cess with autocorrelation function $R(\tau)$, where τ is time lag. IS radar data are discrete
76 samples of the autocorrelation function at discrete ranges r_i , times t_j , and lags τ_k . Power
77 spectral density of the scattered signal, which is the Fourier transform of the autocor-
78 relation function, is a known function of plasma parameters (for example Swartz & Far-
79 ley, 1979, and references therein).

80 Typically, plasma parameters are extracted from the autocorrelation function sam-
81 ples by non-linear least-squares methods with optimization techniques such as Levenberg-
82 Marquardt algorithm. Alternatively, Markov chain Monte Carlo methods can be used
83 for parameter extraction (for example Virtanen et al., 2014), although optimization has
84 remained as academic standard in IS analysis.

85 2.1 Gated analysis and full profile analysis

86 IS analysis techniques can be roughly divided into 'gated' and 'full-profile' tech-
87 niques. In gated analysis one runs the fitting process for each range r_i and time t_j in-
88 dependently from the analysis of neighbouring observational volumes. The EISCAT IS
89 analysis tool GUISDAP (Lehtinen & Huuskonen, 1996) makes gated analysis. In full-
90 profile analysis one fits range profiles of plasma parameters. Main benefit of the full-profile
91 analysis is the possibility to include prior information of plasma parameter altitude pro-
92 files.

93 In its most general form the full-profile analysis performs also deconvolution of lag
94 profiles (Holt et al., 1992; Hysell et al., 2008). A simpler approach is to use phase-coding,
95 for example alternating codes (Lehtinen & Häggström, 1987), and to decode the auto-
96 correlation function samples into high resolution before the plasma parameter fit (Lehtinen
97 et al., 1996). The two-stepped approach can be accomplished with arbitrary transmis-
98 sion modulations if the deconvolution is performed by statistical inversion (Virtanen et
99 al., 2008, 2009). It is technically possible to add prior information already in the lag pro-
100 file inversion step, but expressing the prior in terms of the actual plasma parameters is
101 difficult in this approach.

102 2.2 Bayesian filtering and smoothing

103 Bayesian filtering (for example Särkkä, 2013) is a class of methods for estimating
104 the state of a system from noisy indirect measurements. In IS analysis the state of the
105 system reduces to point estimates of plasma parameter values and their standard devi-
106 ations, while the indirect measurements are the observed autocorrelation function sam-
107 ples \mathbf{R} .

The filtering consists of a sequence of *prediction* and *update* steps. The sequence starts from an initial set of parameters \mathbf{x}_1^- and its covariance matrix \mathbf{P}_1^- , which form our prior understanding of the unknown parameters at time t_1 . Autocorrelation function sam-

ples \mathbf{R}_1 are then used to update the prior model into our best estimates of the parameters and their covariance at time t_1 , \mathbf{x}_1 and \mathbf{P}_1 . The update step is accomplished using a *measurement model* M ,

$$\mathbf{x}_1 = M(\mathbf{x}_1^-, \mathbf{P}_1^-, \mathbf{R}_1). \quad (1)$$

The update step is followed by a prediction step, in which \mathbf{x}_1 and \mathbf{P}_1 are combined with our best understanding of dynamics of the system to create our best prediction of the parameters and their covariance at time t_2 , \mathbf{x}_2^- and \mathbf{P}_2^- . The prediction step is accomplished using a *dynamic model* D ,

$$\mathbf{x}_2^- = D(\mathbf{x}_1, \mathbf{P}_1). \quad (2)$$

Measurements from time t_2 are then used to update the prediction into the final estimates \mathbf{x}_2 and \mathbf{P}_2 , etc.

The simplest 'dynamic' model is to assume that the parameter values at subsequent time steps are close to each other, which reduces the prediction step into

$$\mathbf{x}_j^- = \mathbf{x}_{j-1}, \quad (3)$$

$$\mathbf{P}_j^- = \mathbf{P}_{j-1} + \mathbf{Q}, \quad (4)$$

where \mathbf{Q} is the *system noise covariance matrix*. The larger values \mathbf{Q} has in its diagonal, the smaller is the correlation between subsequent state estimates and the larger is the *filter gain*.

Bayesian filtering allows one to recursively estimate unknowns using the whole time history of measurements. In Bayesian smoothing the idea is extended to use of also 'future' measurements. Bayesian smoothing reduces variances of the unknown parameters and guarantees that equal amount of information from 'past' and 'future' measurements is included in each estimate of the unknowns. This removes a time shift that may be produced by a low-gain filter.

If the dynamic and measurement models are linear functions, Bayesian smoothing can be implemented as a recursive smoothing step called *Rauch-Tung-Striebel* (RTS) smoother (Rauch, 1963). The smoothing recursion runs backwards in time using equations

$$\mathbf{G}_j = \mathbf{P}_j \mathbf{D}_j^T (\mathbf{P}_{j+1}^-)^{-1}, \quad (5)$$

$$\mathbf{x}_j^s = \mathbf{x}_j + \mathbf{G}_j (\mathbf{x}_{j+1}^s - \mathbf{x}_{j+1}^-), \quad (6)$$

$$\mathbf{P}_j^s = \mathbf{P}_j + \mathbf{G}_j (\mathbf{P}_{j+1}^s - \mathbf{P}_{j+1}^-) \mathbf{G}_j^T, \quad (7)$$

where \mathbf{D}_j is the theory matrix of the linear dynamic model D and the superscript T denotes matrix transpose. \mathbf{x}_j^s and \mathbf{P}_j^s form the Bayesian smoothing solution of the problem.

2.3 Correlation priors

Correlation priors (Roininen et al., 2011) allow one to model mutual covariances of the unknowns of an inverse problem in a well controlled way. Assuming that our prior belief of the unknowns \mathbf{x} is \mathbf{x}_p , the prior can be expressed as a linear inverse problem

$$\mathbf{m}_p = \begin{pmatrix} \mathbf{x}_p \\ \mathbf{0} \\ \mathbf{0} \end{pmatrix} = \mathbf{A}_p \mathbf{x} + \boldsymbol{\varepsilon}_p = \begin{pmatrix} \mathbf{A}_{p,0} \\ \mathbf{A}_{p,1} \\ \mathbf{A}_{p,2} \end{pmatrix} \mathbf{x} + \begin{pmatrix} \boldsymbol{\varepsilon}_{p,0} \\ \boldsymbol{\varepsilon}_{p,1} \\ \boldsymbol{\varepsilon}_{p,2} \end{pmatrix}, \quad (8)$$

where \mathbf{x}_p are prior values of the unknown parameters and $\boldsymbol{\varepsilon}_p$ are discrete white noise with variances given in (18), (19), and (20). The theory matrix \mathbf{A}_p is constructed from ze-

roth, first and second order differences $\mathbf{A}_{p,0}$, $\mathbf{A}_{p,1}$, and $\mathbf{A}_{p,2}$, as explained below. Covariance and mean of the prior can be solved from (8) as

$$\Sigma'_p = (\Omega_p)^{-1} = (\mathbf{A}_p^T \Sigma_p^{-1} \mathbf{A}_p)^{-1}, \quad (9)$$

$$\mathbf{x}'_p = \Sigma'_p \mathbf{A}_p^T \Omega_p \mathbf{m}_p, \quad (10)$$

where Σ_p is the error covariance of ε_p , Ω_p is the precision matrix, \mathbf{x}'_p is the final prior mean, and Σ'_p is its error covariance matrix. It is important to notice that the initial profile is smoothed by the correlations and $\mathbf{x}'_p \neq \mathbf{x}_p$. In high-dimensional problems it is important that Ω_p is a sparse matrix (Norberg et al., 2018).

The zeroth order part of the prior is

$$\mathbf{A}_{p,0} = \mathbf{I}, \quad (11)$$

$$\Sigma_{p,0} = \text{diag}(\sigma_{p,0,1}^2, \sigma_{p,0,2}^2, \dots, \sigma_{p,0,N}^2), \quad (12)$$

where the diagonal error covariance matrix $\Sigma_{p,0}$ contains the prior variances of \mathbf{x}_p . The first order terms are

$$\mathbf{A}_{p,1} = \begin{pmatrix} 1 & -1 & 0 & \dots & 0 & 0 \\ 0 & 1 & -1 & \dots & 0 & 0 \\ 0 & 0 & 1 & \dots & 0 & 0 \\ \vdots & \vdots & \vdots & \ddots & \vdots & \vdots \\ 0 & 0 & 0 & \dots & 1 & -1 \end{pmatrix}, \quad (13)$$

$$\Sigma_{p,1} = \text{diag}(\sigma_{p,1,1}^2, \sigma_{p,1,2}^2, \dots, \sigma_{p,1,N-1}^2), \quad (14)$$

and the second order terms are

$$\mathbf{A}_{p,2} = \begin{pmatrix} 1 & -2 & 1 & 0 & \dots & 0 & 0 & 0 \\ 0 & 1 & -2 & 1 & \dots & 0 & 0 & 0 \\ 0 & 0 & 1 & -2 & \dots & 0 & 0 & 0 \\ \vdots & \vdots & \vdots & \vdots & \ddots & \vdots & \vdots & \vdots \\ 0 & 0 & 0 & 0 & \dots & 1 & -2 & 1 \end{pmatrix}, \quad (15)$$

$$\Sigma_{p,2} = \text{diag}(\sigma_{p,2,1}^2, \sigma_{p,2,2}^2, \dots, \sigma_{p,2,N-2}^2). \quad (16)$$

The full prior covariance matrix Σ_p is

$$\Sigma_p = \begin{pmatrix} \Sigma_{p,0} & \mathbf{0} & \mathbf{0} \\ \mathbf{0} & \Sigma_{p,1} & \mathbf{0} \\ \mathbf{0} & \mathbf{0} & \Sigma_{p,2} \end{pmatrix}. \quad (17)$$

Variances of the zeroth, first and second order terms are (Roininen et al., 2011),

$$\sigma_{p,0,i}^2 = c_0^{-1} \alpha_i \ell_i / \Delta h_i, \quad (18)$$

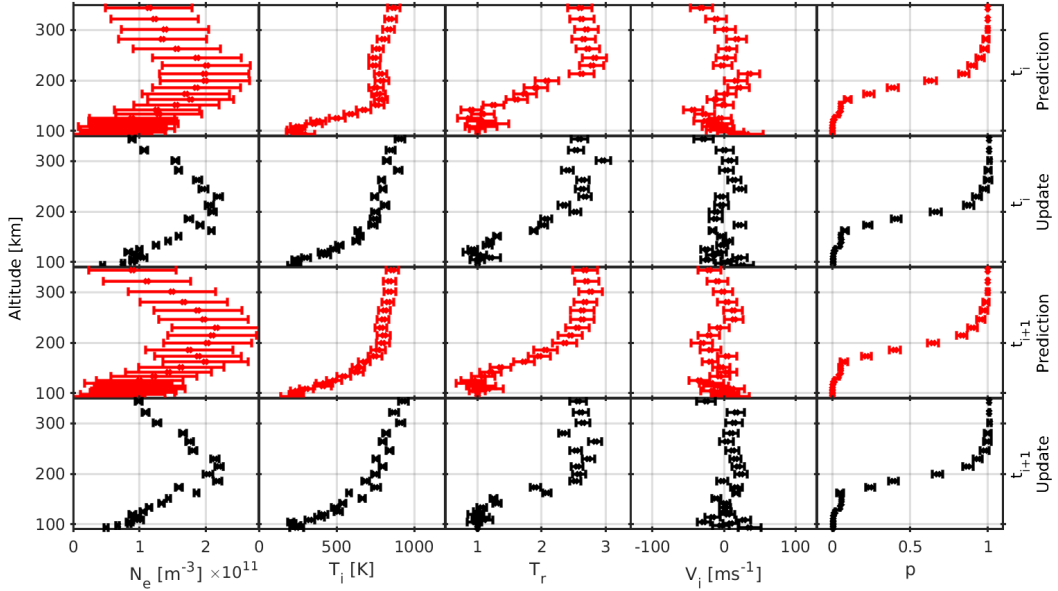
$$\sigma_{p,1,i}^2 = c_1^{-1} \alpha_i \Delta h_i / \ell_i = c_0 / c_1 \sigma_{p,0,i}^2 (\Delta h_i / \ell_i)^2, \quad (19)$$

$$\sigma_{p,2,i}^2 = c_2^{-1} \alpha_i (\Delta h_i / \ell_i)^3 = c_0 / c_2 \sigma_{p,0,i}^2 (\Delta h_i / \ell_i)^4, \quad (20)$$

where α_i is *correlation power* in the $i^{(\text{th})}$ range gate, Δh_i is width of the $i^{(\text{th})}$ range gate, and ℓ_i is the corresponding *correlation length*. The correlation lengths define how smooth the profile is, and the correlation power defines width of the prior distribution. The constants c_0 , c_1 , c_2 define shape of the final covariance structure. For example, $c_0 = 1$, $c_1 = 1/2$, $c_2 = 1/8$ produces a Gaussian covariance. The model variances depend on the discretization and correlation length in a way that makes the model essentially grid-independent.

3 BAFIM implementation

We have implemented an IS analysis tool based on Bayesian filtering in time and correlation priors in range as an additional *Bayesian filtering module* (BAFIM) to the



134 **Figure 1.** Prediction and update steps of BAFIM. Predicted altitude profiles of N_e , T_i , T_r , V_i ,
 135 and p at time t_i (first row), updated profiles at t_i (second row), predicted profiles at t_{i+1} (third
 136 row), and updated profiles at t_{i+1} .

GUISDAP IS analysis tool (Lehtinen & Huuskonen, 1996). We assume a five parameter fit of electron number density N , ion temperature T , ion-to-electron temperature ratio E , line-of-sight plasma velocity V and ion composition $O = [O^+]/N$, where O^+ is the O^+ ion number density. We use the alternative notation ($N=N_e$, $T=T_i$, $E=T_r$, $V=V_i$, $O=p$) in this section to simplify the equations. The vector of plasma parameters at time step j is

$$\mathbf{x}_j = (\mathbf{N}_j, \mathbf{T}_j, \mathbf{E}_j, \mathbf{V}_j, \mathbf{O}_j)^T, \quad (21)$$

where \mathbf{N}_j is the electron density profile in range gates $i = 1, \dots, M$,

$$\mathbf{N}_j = (N_{1,j}, N_{2,j}, \dots, N_{M,j}), \quad (22)$$

and the vectors of the other parameters are defined similarly.

The analysis starts from an initial guess of the plasma parameters at time t_1 , \mathbf{x}_1^- , and their covariance \mathbf{P}_1^- . The parameters \mathbf{x}_1^- are from the International Reference Ionosphere (IRI) model (Bilitza et al., 2017), and \mathbf{P}_1^- is a diagonal matrix with variances equal to the *process noise variances*, defined in (35), in its diagonal. The parameters \mathbf{x}_1^- and their variances $\sigma_1^{2-} = \text{diag}(\mathbf{P}_1^-)$ are used as a prior in a normal GUISDAP fit to measurements \mathbf{R}_1 . The GUISDAP fit is the update step of the Bayesian filter. The gated GUISDAP analysis does not produce a full error covariance matrix of \mathbf{x}_1 , but the error covariance matrix \mathbf{P}_1 contains mutual correlations of plasma parameters in each range gate.

After the first time step, priors for the following GUISDAP fits are not taken from the IRI model, but the fit results from t_1 are used to predict the parameters and their covariance at t_2 . The predicted values \mathbf{x}_2^- and diagonal of \mathbf{P}_2^- are used as prior mean and variance to fit \mathbf{x}_2 and \mathbf{P}_2 to measurements \mathbf{R}_2 , \mathbf{x}_2 and \mathbf{P}_2 are used to calculate the predicted \mathbf{x}_3^- and \mathbf{P}_3^- , etc. The analysis steps are illustrated in Figure 1, whose first row shows predicted altitude profiles of $N=N_e$, $T=T_i$, $E=T_r$, $V=V_i$, and $O=p$ at time t_i . The predictions are used as priors in a GUISDAP fit, which produces the updated profiles

on the second row. The profiles on the second row are used to predict the parameter profiles at time t_{i+1} (third row), the prediction is used as a prior when fitting the parameters at time t_{i+1} (fourth row), etc. Correlations in range are lost and reintroduced in each update and prediction step, correspondingly. This allows us to use the computationally light-weight gated analysis, and the approach is acceptable if the plasma parameters do not change much during a time step.

In the prediction step, a correlation prior is used to create smooth plasma parameter profiles. The measurements \mathbf{x}_1 and their covariance \mathbf{P}_1 are used as the zeroth order terms in (8),

$$\mathbf{x}_p = \mathbf{x}_1, \quad (23)$$

$$\Sigma_{p,0} = \mathbf{P}_1. \quad (24)$$

The first and second order differences in (8) are then formed for each plasma parameter separately. Variances of the plasma parameters $\mathbf{x}_1 = (\mathbf{N}_1, \mathbf{T}_1, \mathbf{E}_1, \mathbf{V}_1, \mathbf{O}_1)^T$ are

$$\sigma_{p,0}^2 = (\sigma_{N,0}^2, \sigma_{T,0}^2, \sigma_{E,0}^2, \sigma_{V,0}^2, \sigma_{O,0}^2)^T = \text{diag}(\mathbf{P}_1). \quad (25)$$

The first order difference matrices (13) for each parameter are identical $M \times M - 1$ matrices, $\mathbf{A}_{N,1} = \mathbf{A}_{T,1} = \mathbf{A}_{E,1} = \mathbf{A}_{V,1} = \mathbf{A}_{O,1}$, and the full first order difference matrix is the block diagonal matrix

$$\mathbf{A}_{p,1} = \begin{pmatrix} \mathbf{A}_{N,1} & \mathbf{0} & \mathbf{0} & \mathbf{0} & \mathbf{0} \\ \mathbf{0} & \mathbf{A}_{T,1} & \mathbf{0} & \mathbf{0} & \mathbf{0} \\ \mathbf{0} & \mathbf{0} & \mathbf{A}_{E,1} & \mathbf{0} & \mathbf{0} \\ \mathbf{0} & \mathbf{0} & \mathbf{0} & \mathbf{A}_{V,1} & \mathbf{0} \\ \mathbf{0} & \mathbf{0} & \mathbf{0} & \mathbf{0} & \mathbf{A}_{O,1} \end{pmatrix}. \quad (26)$$

Variances of the first order terms are calculated from (19). First order variances for electron density are

$$\sigma_{N,1,i}^2 = c_0/c_1 \sigma_{N,0,i}^2 (\Delta h_i/\ell_{N,i})^2, \quad (27)$$

and variances of the other parameters are calculated in a similar manner. The first order covariance matrix is the diagonal matrix

$$\Sigma_{p,1} = \text{diag}(\sigma_{N,1}^2, \sigma_{T,1}^2, \sigma_{E,1}^2, \sigma_{V,1}^2, \sigma_{O,1}^2). \quad (28)$$

The second order differences and their variances are formed in a similar manner. As a result, we have a matrix equation of the form (8), from which parameter profiles smoothed in range, \mathbf{x}' , and their covariance, Σ' , can be solved using (9) and (10).

The smoothed parameter profiles \mathbf{x}' are used as the prediction for time step t_2 ,

$$\mathbf{x}_2^- = \mathbf{x}', \quad (29)$$

and the predicted covariance is the sum of the covariance of \mathbf{x}' and a process noise covariance \mathbf{Q} ,

$$\mathbf{P}_2^- = \Sigma' + \mathbf{Q}. \quad (30)$$

The process noise covariance is a diagonal $5M \times 5M$ matrix with a different variance for each plasma parameter (35) in its diagonal,

$$\mathbf{Q} = \text{diag}(q_N, \dots, q_N, q_T, \dots, q_T, q_E, \dots, q_E, q_V, \dots, q_V, q_O, \dots, q_O). \quad (31)$$

The RTS smoother is implemented in BAFIM as a post-processing step. Since only the first $5M$ elements of the vector \mathbf{m}_p are nonzero in (8) and (10), the matrix \mathbf{D} in (5) consists of the first $5M$ columns of the $5M \times (15M - 3)$ matrix

$$\mathbf{D}' = \Sigma_s \mathbf{A}_p^T \Omega_p. \quad (32)$$

163 The RTS smoother is only a linear approximation, but the approximation is reasonable
 164 if the time steps are short enough to keep changes in plasma parameters small in between
 165 subsequent time steps.

The correlation lengths ℓ_i are proportional to the plasma scale height

$$H_i = \frac{k_B T_i (1 + E_i)/2}{m_i g_i}, \quad (33)$$

calculated from the IRI model parameters. Here k_B is the Boltzmann constant, m_i is the mean ion mass, g_i is the acceleration of gravity, and the subscript i refers to the $i^{(th)}$ range gate. The correlation lengths of N are

$$\ell_{N,i} = s_N^h H_i, \quad (34)$$

166 where s_N^h is a constant, and the correlation lengths of the other parameters are defined
 167 in a similar manner.

168 In the correlation prior, covariance of the zeroth order terms is the posterior co-
 169 variance $\Sigma_{p,0} = \mathbf{P}_1$, and variances of the first and second order terms are proportional
 170 to ℓ_i^{-2} and ℓ_i^{-4} , respectively. Thus, at the limit of small correlation lengths ℓ_i , the smoothed
 171 profile \mathbf{x}' approaches the fitted profile \mathbf{x}_1 , and the covariance Σ' approaches \mathbf{P}_1 . BAFIM
 172 can thus be run without the smoothing in range if the correlation lengths ℓ_i are small,
 173 i.e. the constants s^h are small.

The process noise variances q_N, q_T, q_E, q_V, q_O are proportional to the time step duration,

$$q_N = (s_N^t)^2 \Delta t, \quad (35)$$

174 etc. Each parameter is fitted within an altitude interval $[h_{min}, h_{max}]$, below h_{min} and
 175 above h_{max} the parameter is fixed to the IRI model value with a small variance. The
 176 heights $h_{min,N}, h_{max,N}, h_{min,T}, h_{max,T}, \dots$, the constants $s_N^h, s_T^h, s_E^h, s_V^h, s_O^h$, and the
 177 constants $s_N^t, s_T^t, s_E^t, s_V^t, s_O^t$ are user inputs and may vary from one analysis run to another.

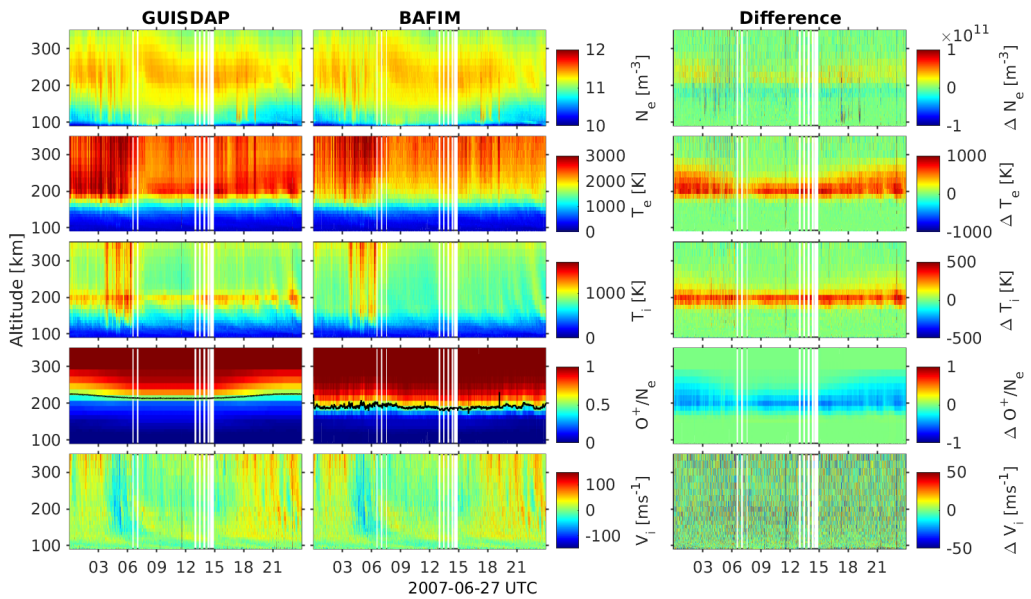
179 4 Plasma parameter fits with BAFIM

180 In this section we demonstrate plasma parameter fits with BAFIM in two use cases,
 181 ion composition fits in the F_1 region and high-resolution E region analysis during au-
 182 roral electron precipitation. We use field-aligned observations from the EISCAT Sval-
 183 bard radar (ESR) and the EISCAT UHF radar. We consider fits of electron density (N_e),
 184 ion temperature (T_i), ion-to-electron temperature ratio (T_r), line-of-sight plasma bulk
 185 velocity (V_i), and ion composition ($p = [O^+]/N_e$). In the results we show the electron
 186 temperature $T_e = T_i \cdot T_r$ instead of T_r . While the assumption of smoothness in range
 187 is necessary in the selected demonstrations, we emphasize that BAFIM can be used also
 188 without this assumption, for example to improve time resolution of four-parameter fits
 189 in low-elevation or bistatic observations. In this section, standard GUISDAP fits and GUI-
 190 S DAP fits with BAFIM are referred to as 'GUISDAP' and 'BAFIM', correspondingly.

191 Both ESR and UHF data are from experiments that use alternating codes (Lehtinen
 192 & Häggström, 1987). The ESR 'ipy' experiment uses a 30-bit code sequence with $30 \mu\text{s}$
 193 bit length and the data are decoded to 2.25 km resolution. The UHF 'arc1' experiment
 194 uses a 64-bit code sequence with $6 \mu\text{s}$ bit length and the data are decoded to 900 m res-
 195 olution. In high signal-to-noise conditions GUISDAP may underestimate plasma param-
 196 eter variances because it neglects correlations between autocorrelation function samples
 197 (Huuskonen & Lehtinen, 1996). Both experiments use randomized (Lehtinen et al., 1997)
 198 codes to reduce the correlations. If highly correlated data were analysed with BAFIM,
 199 smoothing in time and range would be reduced due to the underestimation of errors in
 200 the GUISDAP fits.

202 **Table 1.** BAFIM settings used in the data analysis. N_e , T_i , T_r , and V_i are fitted at all altitudes
 203 above h_{min} . p is not fitted at all in the E region analysis of the UHF data. The constants s^h and
 204 s^t are scaling factors that control smoothness of the solutions in range and time, respectively, as
 205 explained in Section 3.

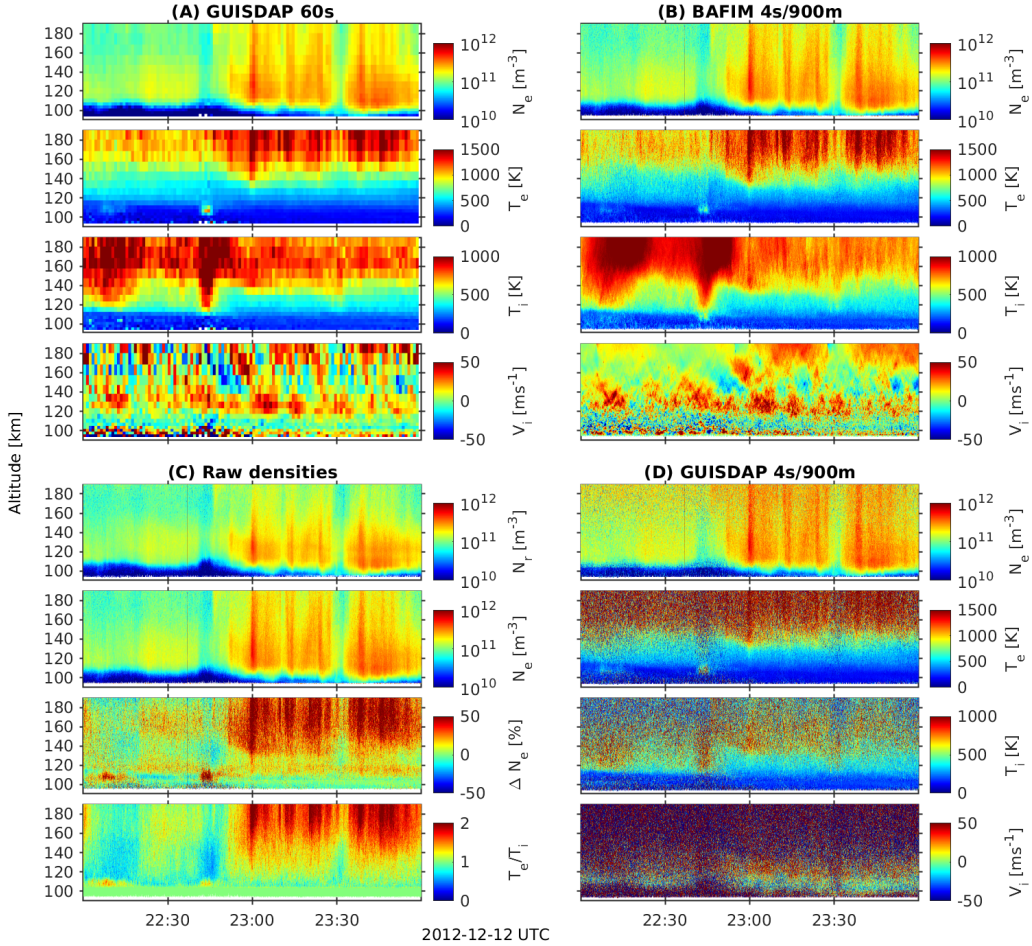
	ESR 27 June 2007				UHF 12 December 2012			
	s^h	s^t	h_{min} (km)	h_{max} (km)	s^h	s^t	h_{min} (km)	h_{max} (km)
N_e	0.1	$2.5 \cdot 10^{10} \text{ m}^{-3} \text{s}^{-1/2}$	0	-	1.0	$2.5 \cdot 10^{11} \text{ m}^{-3} \text{s}^{-1/2}$	0	-
T_i	0.3	$10 \text{ Ks}^{-1/2}$	80	-	0.2	$30 \text{ Ks}^{-1/2}$	80	-
T_r	0.3	$0.05 \text{ s}^{-1/2}$	103	-	0.4	$0.1 \text{ s}^{-1/2}$	103	-
V_i	0.2	$2.5 \text{ ms}^{-3/2}$	80	-	0.1	$5 \text{ ms}^{-3/2}$	80	-
p	0.2	$0.003 \text{ s}^{-1/2}$	150	320	-	-	0	0



206 **Figure 2.** Ion composition analysis. GUISDAP four-parameter fit with 60 s resolution (left),
 207 five-parameter BAFIM fit with 6 s time steps (middle), and difference of these two (GUISDAP -
 208 BAFIM) (right). In the default GUISDAP fit the ion composition is from the IRI model.

201 4.1 Ion composition fits

209 Ion frictional heating occurs when an electric field drives the ionospheric plasma
 210 through the neutral atmosphere and the ion gas is heated in collisions with neutral par-
 211 ticles. The heating may affect F₁ region ion composition, because reaction rates of some
 212 important charge-exchange reactions depend on temperature, and expansion of the neu-
 213 tral atmosphere may increase neutral N₂ concentration in the F region (Kelly & Wick-
 214 war, 1981). Deviations from the IRI ion composition may bias F₁ region ion tempera-
 215 ture estimates in four-parameter GUISDAP fits of N_e , T_e , T_i and V_i . An example of such
 216 an event is shown on the left in Figure 2, where four-parameter GUISDAP fit results with
 217 60 s resolution are shown for 24 hours of ESR data. Ion temperature (third panel on the
 218 left) has an artificial local maximum around 200 km altitude, where IRI predicts too much
 219 molecular ions (fourth panel).



234 **Figure 3.** High-resolution E region analysis. (A) GUISDAP fit with 60 s time resolution and
 235 range resolution varying from 3 km to 13 km, (B) BAFIM fit with 4 s/900 m steps, (C) N_r ,
 236 BAFIM-fitted N_e , relative difference $\Delta N_e = (N_e - N_r)/N_r$, and BAFIM T_e/T_i , (D) GUISDAP fit
 237 with 4 s/900 m resolutions.

220 In five-parameter BAFIM fit of the same data (Figure 2, middle panels), also the
 221 ion composition p is fitted, and the analysis proceeds with 6 s time steps. Other BAFIM
 222 settings are listed in Table 1. The artificial ion temperature maximum, which is visible
 223 in the GUISDAP fit, is not produced in the BAFIM fit. The transition altitude, where
 224 number density of molecular ions is equal to O^+ density ($p = 50\%$, black lines in the
 225 fourth panels), is generally lower than in the IRI model. Difference of the two fit results
 226 (GUISDAP - BAFIM) is shown on the right in Figure 2, where one can see how the dif-
 227 ference in p affects also T_i , T_e and even N_e profiles. While the artefact around 200 km
 228 altitude was removed by BAFIM, the true ion frictional heating events between 4 and
 229 7 UT, as well as the weaker T_i enhancements after 15 UT, are reproduced by BAFIM,
 230 demonstrating its ability to maintain true ion temperature maxima. We note that our
 231 results are very similar with those of Blelly and van Eyken (2010), who used the same
 232 data to demonstrate a full-profile analysis technique based on ion energy equations.

233 **4.2 High-resolution observations of auroral electron precipitation**

238 IS radars can detect impact ionization and electron heating caused by auroral elec-
 239 tron precipitation. While existing high-latitude IS radars can typically reach a time reso-
 240 lution of some tens of seconds in the four-parameter fits of N_e , T_i , T_r , and V_i , optical
 241 observations show that the precipitation may change substantially in a few seconds and
 242 even below (for example Dahlgren et al., 2016). High-resolution E region observations
 243 often rely on raw electron densities (for example Semeter & Kamalabadi, 2005; Dahlgren
 244 et al., 2011; Virtanen et al., 2018), which are calculated assuming $T_e = T_i$. However,
 245 this assumption may not be justified, since the precipitation heats the electron gas.

246 Figure 3 shows plasma parameter fit results from three different analysis runs of
 247 an EISCAT UHF radar measurement on 12 December 2012: (A) a four-parameter GUIS-
 248 DAP fit with 60 s time resolution and range resolution varying from 3 km to 13 km, (B)
 249 a BAFIM fit with 4 s/900 m steps, and (D) a GUISDAP fit with 4 s/900 m resolution.
 250 BAFIM settings are listed in Table 1. While plasma parameters from the GUISDAP fit
 251 are extremely noisy with the 4 s/900 m resolution, the BAFIM fit produces temperatures
 252 and velocities that match well with the standard coarse-resolution fit (for example, com-
 253 pare T_i and V_i in panels (A), (B), and (D)).

254 Importance of the temperature fit is demonstrated in Figure 3 (C), which shows
 255 raw electron density N_r , BAFIM-fitted N_e , relative difference $(N_e - N_r)/N_r$, and the
 256 temperature ratio T_e/T_i . The raw densities are clear underestimates after 22:50 UT, when
 257 electron precipitation heats the electron gas and $T_e > T_i$. This effect was neglected for
 258 example in Virtanen et al. (2018), because the high-resolution four-parameter fits were
 259 practically impossible.

260 **5 Discussion**

261 BAFIM is the first implementation of Bayesian filtering to IS plasma parameter
 262 fits. In this section we discuss some important properties of BAFIM and potential fu-
 263 ture improvements.

264 **5.1 Resolutions of BAFIM fit results**

265 While the BAFIM analysis proceeds with short steps in range and time, each fit
 266 result may contain information from considerably longer intervals because the steps are
 267 correlated. One should thus make a clear difference between the effective resolutions –
 268 the intervals in range and time which make significant contributions to the fit result –
 269 and the step sizes. The effective resolutions are not constants, but they depend on the
 270 amount of information gained from each individual measurement. Effective resolutions
 271 of each parameter at each altitude may be tuned separately by adjusting the correspond-
 272 ing process noise variances and correlation lengths. Effective resolutions of N_e are typ-
 273 ically kept very close to the step sizes, while coarser effective resolutions are accepted
 274 for the other parameters to reach an acceptable statistical accuracy.

275 **5.2 Tuning and validating BAFIM**

276 Tuning the process noise variances and correlation lengths of BAFIM may be non-
 277 trivial, since the correlations in time allow part of the prior information introduced with
 278 the correlation priors to be passed from one time step to another. Any change in pro-
 279 cess noise variance must thus be compensated with a corresponding change in corre-
 280 lation length to keep the effective smoothing in range unchanged. In addition, changing
 281 the process noise and correlation length of one plasma parameter may affect the others
 282 due to error correlations.

In this paper, BAFIM was tuned to produce practically uncorrelated electron densities, while correlation lengths and process noise variances of the other parameters were selected in such a way that noise level of the fitted parameters roughly matched with the default GUISDAP fits with 60 s resolution. The only physics-based part of the model are the correlation lengths, which are proportional to the plasma scale heights. Physics-based, automatic ways to tune the filter will be topics of future works. Alternative ways to tune the filter would be to derive theoretical limits for gradients in space and time, or to extract information on the correlation structures from existing measurements. Correlation structures of mesospheric winds have been extracted from meteor radar observations by Vierinen et al. (2019), and a similar work for incoherent scatter radars could be possible.

Validation of BAFIM results, the ion composition fits in particular, is a challenging task due to lack of measurements from other instruments. Observations of F_1 region ion composition are mainly from rockets, and the rocket observation would need to be from vicinity of the radar beam to enable reasonable comparisons. Alternatively, one could analyse simulated radar data corresponding a realistic model ionosphere. Such simulations would be possible for example with the simISR tool (Swoboda et al., 2017).

5.3 Ion composition fits

In the ion composition fits a small process noise variance q_O was used for the ion composition and a relatively large variance q_T was used for the ion temperature, which is equivalent with the assumption that ion temperature varies much more rapidly than ion composition. Only slow variations in composition were allowed, because allowing rapid variations in both ion composition and temperature may lead to unrealistic oscillations due to the temperature-ion composition ambiguity. With the selected tuning BAFIM can follow the relatively slow ion composition variations associated with the large scale convection electric field, but rapid variations caused, for example, by small scale electric fields around auroral arcs are challenging.

Time resolution of the composition fits could be improved if physics-based models were included in the prediction step. One could either model the temperature profiles or include a chemistry model that solves temperature-dependent compositions. The temperature profiles could be modeled, for example, with the techniques of Zettergren et al. (2011) and Blelly and van Eyken (2010), while chemistry modeling could be adopted for example from Richards and Voglozin (2011). Also D region ion composition and temperatures could be observed if a sufficient model, for example the Sodankylä Ion and Neutral Chemistry (SIC) model (Turunen et al., 2016) was used.

5.4 EISCAT_3D

EISCAT_3D (McCrea et al., 2015) is the next-generation geospace radar system currently being built in northern Norway, Sweden, and Finland. The radar will provide an order-of-magnitude improvement in measurement speed, and it will be the first multistatic, multibeam incoherent scatter radar system. EISCAT_3D will be able to conduct volumetric observations, including 3D observations of plasma flows.

If BAFIM-like analysis was applied to field-aligned EISCAT_3D measurements, the order-of-magnitude improvement would mean sub-second time steps in four-parameter fits, and resolutions sufficient for rapidly varying conditions in association with aurora in ion composition fits. The volumetric observations would allow one to implement 3D models of the ionosphere in the prediction step. An EISCAT_3D analysis tool could be designed for the volumetric observations and could make optimal use of the multistatic, multibeam data, following the idea of Virtanen et al. (2014).

331 **6 Conclusions**

332 We have introduced an incoherent scatter analysis technique that allows us to con-
 333 trol plasma parameter gradients in both time and space using Bayesian filtering and cor-
 334 relation priors. The technique is implemented as a Bayesian filtering module (BAFIM)
 335 in the GUISDAP analysis package. BAFIM allows us to fit F_1 region ion composi-
 336 tions and transition altitudes, and to include ion and electron temperatures in high res-
 337 olution plasma parameter fits, in field-aligned incoherent scatter measurements. Improve-
 338 ments provided by the new analysis tool were demonstrated with EISCAT radar data,
 339 including fits of F_1 region ion composition and high-resolution E region plasma param-
 340 eter fits during short-lived auroral precipitation events. The technique could be extended
 341 to volumetric, multistatic observations of the EISCAT_3D radar and supplemented with
 342 ion chemistry models.

343 **Acknowledgments**

344 This work is supported by the Academy of Finland, application numbers 285474, 326240,
 345 and 301542, and the Kvantum institute of the University of Oulu. EISCAT is an inter-
 346 national association supported by research organisations in China (CRIRP), Finland (SA),
 347 Japan (NIPR and STEL), Norway (NFR), Sweden (VR), and the United Kingdom (NERC).
 348 The EISCAT data and the GUISDAP software are available for download from the EIS-
 349 CAT web page (<http://www.eiscat.se>). BAFIM is available at <https://doi.org/10.5281/zenodo.4033904>.

350 **References**

- 351 Bilitza, D., Altadill, D., Truhlik, V., Shubin, V., Galkin, I., Reinisch, B., & Huang,
 352 X. (2017). International Reference Ionosphere 2016: From ionospheric cli-
 353 mate to real-time weather predictions. *Space Weather*, 15(2), 418-429. doi:
 354 10.1002/2016SW001593
- 355 Blelly, P.-L., & van Eyken, A. P. (2010). A new analysis method for deter-
 356 mining polar ionosphere and upper atmosphere characteristics from ESR
 357 data: Illustration with IPY period. *J. Geophys. Res.*, 115, A09322. doi:
 358 10.1029/2009JA014876
- 359 Cabrit, B., & Kofman, W. (1996). Ionospheric composition measurement by EIS-
 360 CAT using a global fit procedure. *Ann. Geophys.*, 14, 1496-1505. doi: 10.1007/
 361 s00585-996-1496-2
- 362 Dahlgren, H., Gustavsson, B., Lanchester, B. S., Ivchenko, N., Brändström, U.,
 363 Whiter, D. K., ... Marklund, G. (2011). Energy and flux variations across thin
 364 auroral arcs. *Ann. Geophys.*, 29, 1699-1712. doi: 10.5194/angeo-29-1699-2011
- 365 Dahlgren, H., Lanchester, B. S., Ivchenko, N., & Whiter, D. K. (2016). Elec-
 366 trodynamics and energy characteristics of aurora at high resolution by op-
 367 tical methods. *J. Geophys. Res. Space Physics*, 121, 5966-5974. doi:
 368 10.1002/2016JA022446
- 369 Häggström, I., & Collis, P. N. (1990). Ion composition changes during F-region den-
 370 sity depletions in the presence of electric fields at auroral latitudes. *J. Atmos.*
 371 *Terr. Phys.*, 52(6-8), 519-529. doi: 10.1016/0021-9169(90)90050-W
- 372 Holt, J. M., Rhoda, D. A., Tetenbaum, D., & van Eyken, A. P. (1992). Optimal
 373 analysis of incoherent scatter radar data. *Radio Sci.*, 27(3), 435-447. doi: 10
 374 .1029/91RS02922
- 375 Huuskonen, A., & Lehtinen, M. S. (1996, January). The accuracy of incoherent scat-
 376 ter measurements: error estimates valid for high signal levels. *Journal of At-*
 377 *mospheric and Terrestrial Physics*, 58, 453-463.
- 378 Hysell, D. L., Rodrigues, F. S., Chau, J. L., & Huba, J. D. (2008). Full profile inco-
 379 herent scatter analysis at Jicamarca. *Ann. Geophys.*, 26, 59-75. doi: 10.5194/
 380 angeo-26-59-2008
- 381 Kelly, J. D., & Wickwar, V. B. (1981). Radar measurements of high-latitude ion

- 382 composition between 140 and 300 km altitude. *J. Geophys. Res.*, 86(A9),
 383 7617-7626. doi: 10.1029/JA086iA09p07617
- 384 Lathuillere, C., Lejeune, G., & Kofman, W. (1983). Direct measurements of ion com-
 385 position with EISCAT in high-latitude F_1 region. *Radio Sci.*, 18(6), 887-893.
 386 doi: 10.1029/RS018i006p00887
- 387 Lehtinen, M. S., & Häggström, I. (1987). A new modulation principle for in-
 388 coherent scatter measurements. *Radio Sci.*, 22, 625-634. doi: 10.1029/
 389 RS022i004p00625
- 390 Lehtinen, M. S., & Huuskonen, A. (1996). General incoherent scatter analysis and
 391 GUISDAP. *J. Atmos. Terr. Phys.*, 58, 435-452. doi: 10.1016/0021-9169(95)
 392 00047-X
- 393 Lehtinen, M. S., Huuskonen, A., & Markkanen, M. (1997). Randomization of alter-
 394 nating codes: Improving incoherent scatter measurements by reducing correla-
 395 tions of gated autocorrelation function estimates. *Radio Sci.*, 32, 2271-2282.
 396 doi: 10.1029/97RS02556
- 397 Lehtinen, M. S., Huuskonen, A., & Pirttilä, J. (1996). First experiences of full-profile
 398 analysis with GUISDAP. *Ann. Geophys.*, 14, 1487-1495. doi: 10.1007/s00585
 399 -996-1487-3
- 400 Martínez-Ledesma, M., Quezada, D., & Andrés, M. (2019). Determination of the
 401 Signal Fluctuation Threshold of the Temperature-Ion Composition Ambiguity
 402 Problem Using Monte Carlo Simulations. *J. Geophys. Res. Space Physics*,
 403 124(4), 2897-2919. doi: 10.1029/2018JA026217
- 404 McCrea, I., Aikio, A., Alfonsi, L., Belova, E., Buchert, S., Clilverd, M., ... Vierinen,
 405 J. (2015). The science case for the EISCAT_3D radar. *Prog. Earth Planet. Sc.*,
 406 2(1). doi: 10.1186/s40645-015-0051-8
- 407 Norberg, J., Vierinen, J., Roininen, L., Orispää, M., Kauristie, K., Rideout, W. C.,
 408 ... Lehtinen, M. S. (2018). Gaussian Markov Random Field Priors in Iono-
 409 spheric 3-D Multi-Instrument Tomography. *IEEE Trans. Geosci. Remote
 410 Sens.*, 1-13. doi: 10.1109/TGRS.2018.2847026
- 411 Rauch, H. R. (1963). Solutions to the linear smoothing problem. *IEEE T. Automat.
 412 Contr.*, 8(4), 371-372.
- 413 Richards, P. G., & Voglozin, D. (2011). Reexamination of ionospheric photochem-
 414 istry. *J. Geophys. Res. Space Physics*, 116(A8). doi: 10.1029/2011JA016613
- 415 Roininen, L., Lehtinen, M. S., Lasanen, S., Orispää, M., & Markkanen, M. (2011).
 416 Correlation Priors. *Inverse Problems and Imaging*, 5(1), 167-184. doi: 10
 417 .3934/ipi.2011.5.167
- 418 Särkkä. (2013). *Bayesian Filtering and Smoothing*. Cambridge University Press.
- 419 Semeter, J., & Kamalabadi, F. (2005). Determination of primary electron spec-
 420 tra from incoherent scatter radar measurements of the auroral E region. *Radio
 421 Sci.*, 40, RS2006. doi: 10.1029/2004RS003042
- 422 Swartz, W. E., & Farley, D. T. (1979). A Theory of Incoherent Scattering of
 423 Radio Waves by a Plasma 5. The Use of the Nyquist Theorem in General
 424 Quasi-Equilibrium Situations. *J. Geophys. Res.*, 84(A5), 1930-1932. doi:
 425 10.1029/JA084iA05p01930
- 426 Swoboda, J., Semeter, J., Zettergren, M., & Erickson, P. J. (2017). Observability
 427 of ionospheric space-time structure with ISR: A simulation study. *Radio Sci.*,
 428 52(2), 215-234. doi: 10.1002/2016RS006182
- 429 Turunen, E., Kero, A., Verronen, P. T., Miyoshi, Y., Oyama, S.-I., & Saito, S.
 430 (2016). Mesospheric ozone destruction by high-energy electron precipitation
 431 associated with pulsating aurora. *J. Geophys. Res. Atmos.*, 121, 11852-11861.
 432 doi: 10.1002/2016JD025015
- 433 Vierinen, J., Chau, J. L., Charuvil, H., Urco, J. M., Clahsen, M., Avsarkisov, V.,
 434 ... Volz, R. (2019). Observing mesospheric turbulence with specular meteor
 435 radars: A novel method for estimating second-order statistics of wind velocity.
 436 *Earth and Space Science*, 6(7), 1171-1195. doi: 10.1029/2019EA000570

manuscript submitted to *JGR-Space Physics*

- 437 Virtanen, I. I., Gustavsson, B., Aikio, A. T., Kero, A., Asamura, K., & Ogawa, Y.
438 (2018). Electron Energy Spectrum and Auroral Power Estimation from In-
439 coherent Scatter Radar Measurements. *J. Geophys. Res. Space Physics*, *123*,
440 6865-6887. doi: 10.1029/2018JA025636
- 441 Virtanen, I. I., Lehtinen, M. S., Nygrén, T., Orispää, M., & Vierinen, J. (2008). Lag
442 profile inversion method for EISCAT data analysis. *Ann. Geophys.*, *26*, 571-
443 581. doi: 10.5194/angeo-26-571-2008
- 444 Virtanen, I. I., McKay-Bukowski, D., Vierinen, J., Aikio, A. T., Fallows, R., &
445 Roininen, L. (2014, December). Plasma parameter estimation from multistatic,
446 multibeam incoherent scatter data. *J. Geophys. Res. Space Physics*, *119*(12),
447 10528-10543. doi: 10.1002/2014JA020540
- 448 Virtanen, I. I., Vierinen, J., & Lehtinen, M. S. (2009, July). Phase-coded pulse ape-
449 riodic transmitter coding. *Ann. Geophys.*, *27*, 2799-2811. doi: 10.5194/angeo
450 -27-2799-2009
- 451 Zettergren, M., Semeter, J., Heinselman, C., & Diaz, M. (2011). Incoherent scatter
452 radar estimation of F region ionospheric composition during frictional heating
453 events. *J. Geophys. Res.*, *116*, A01318. doi: 10.1029/2010JA016035